Proposition and Comparison of Several Solutions for High Induced Voltage across Inactive Transmitting coils in a Series-Series Compensation DIPT System

Wassim Kabbara, Mohamed Bensetti, Tanguy Phulpin, Antoine Caillerez, Serge Loudot, Daniel Sadarnac

Proposition and Comparison of Several Solutions for High Induced Voltage across Inactive Transmitting coils in a Series-Series Compensation DIPT System

Wassim KABBARA[1,2], Mohamed BENSETTI[1], Tanguy PHULPIN[1], Antoine CAILLIEREZ[2], Serge LOUDOT[2] and Daniel SADARNAC[1]

[1.] LABORATOIRE DE GENIE ELECTRIQUE ET ELECTRONIQUE DE PARIS, CNRS, CENTRALESUPELEC, SORBONNE UNIVERSITE, UNIVERSITE DE PARIS SACLAY
3 rue Joliot Curie, 91192 Gif-sur-Yvette, France

[2.] RENAULT
1 Avenue du Golf, 78084 Guyancourt, France

E-Mail: wassim.kabbara@centralesupelec.fr
URL: https://www.geeps.centralesupelec.fr

Keywords

«Wireless power transmission», «Robustness», «Resonant converter», «System Integration»

Abstract

Dynamic inductive power transfer technology (DIPT) has recently seen significant development. It is proposed as an alternative solution for increasing the range of electrical vehicles (EV) while decreasing the battery size. Transmitting coils located under the road transfer the power to a receiving coil integrated within the moving EV by inductive coupling. In a (S-S) DIPT system with multiple transmitting coils, a high induced voltage can occur on the adjacent inactive transmitting coils, thus creating numerous risks. This high induced voltage risks reinjecting power to the grid and thus significantly decreases the system's performance and efficiency. In this article, we present and compare several solutions for the high-induced voltage problem. A four-quadrant switch is designed, modeled, and realized based on two technologies: Saturable reactor and IGBT transistors. Then the 4Q-switch solution is compared with the short-circuiting method. Experimental validation is performed using a series-series DIPT platform using a 300 W resistive load with variable frequency control.

Introduction

Electrical vehicles (EVs) are witnessing significant advancement on many levels [1]. One central research area is how to increase an EV's autonomy without increasing its battery's size. Dynamic Inductive Power Transfer (DIPT) has been a technology in development for several years now and is proposed to increase the range of EVs without using bigger batteries [2]–[4]. It consists of multiple transmitting coils embedded in the road, sending energy by magnetic induction to an embedded receiver coil inside the EV, thus charging wirelessly while in motion. According to a case study in Lisbon [5], dynamic wireless charging would enable more drivers to adopt EVs by 13 to 18%. In addition, the study showed that the maximum change experienced by the state of charge of the EV would be reduced by 2/3, confirming that using this technology significantly reduces battery usage.

In DIPT, compensation circuits are often added to the system due to high leakage flux [6]. Symmetrical Series-Series (S-S) compensation topology is often used in EV charging applications due to its high tolerance for coupling variations and higher peak efficiency [7], [8]. Fig. 1-a presents a typical series-series DIPT system with three transmitting coils on the road and one receiving coil in the EV with an equivalent load (R_{Load}).

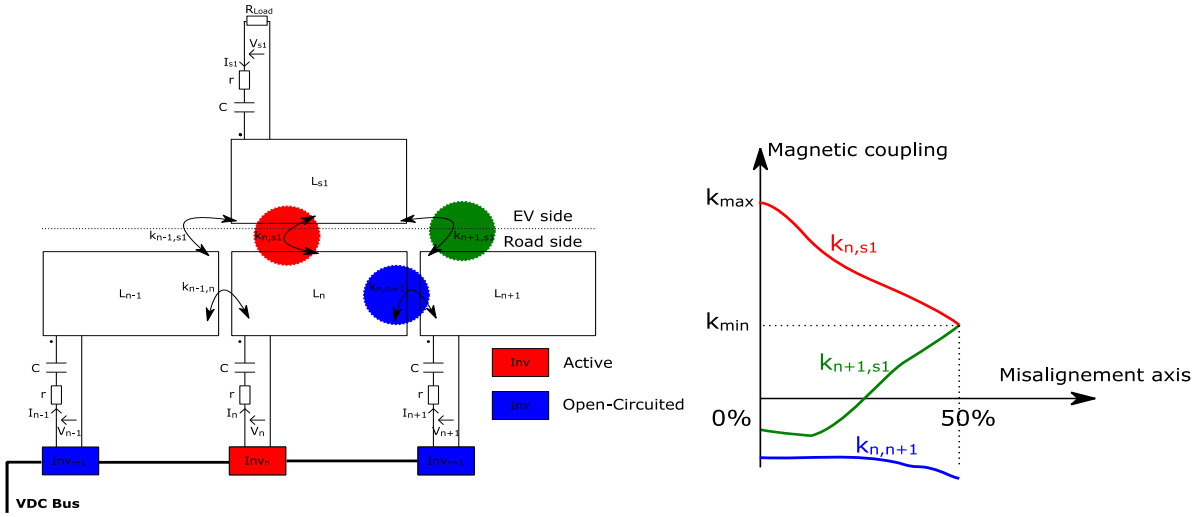

(**a**) (**b**)

Fig. 1: (**a**) Model of a series-series DIPT system with a resistive load RLoad; (**b**) Typical magnetic coupling between transmitting and receiving coils of identical sizes

The electromagnetic leakage fields generated by the active primary and the secondary coils can create a high induced voltage across the neighboring inactive transmitting coils due to magnetic coupling between these coils, as illustrated in Fig. 1-b. This induced voltage increases with the misalignment of the secondary coil. It could become higher than the V_{DC_bus} used on the primary side, thus reinjecting power to the grid and degrading the system's performance and efficiency.

A possible solution for this problem would be spacing the transmitting coils enough to lower the magnetic couplings over the inactive neighboring transmitting coils (ex: $k_{n,n+1}$ & $k_{n+1,s1}$). This would solve the problem but lead to zero power transfer zones. Using one long transmitter coil as proposed in [9] would eliminate this problem; however, it would be difficult to respect the maximum radiated magnetic field around the vehicle as declared by the INCIRP [10]. [11], [12] propose activating and synchronizing multiple transmitting coils. However, the perfect symmetry of the system's magnetic and electrical parameters should be respected. Otherwise, the power transfer would not be stable due to magnetic coupling between transmitters. In [11], [12], the overvoltage problem across the inactive transmitters was not mentioned since they have activated all transmitter coils simultaneously. In [13], a similar synchronization method was adopted, and a solution for the induced voltage across neighboring transmitters was proposed by limiting the reinjected current (80% DC to DC efficiency at 100 W load, 6.78 MHz). In [14], a coil geometry that significantly reduces the magnetic coupling between two adjacent transmitters was proposed. However, this solution does not eliminate the coupling between the secondary coil and the next inactive transmitter ($k_{n+1,s1}$).

This paper proposes using a 4 Quadrant switch in series with the transmitting coils to solve the high induced voltage problem across inactive transmitting coils in a symmetrical series-series compensation network. A 4Q-switch is proposed, and realized based on two technologies: Saturable reactors [15], [16] and IGBT transistors [17], [18]. Then the 4Q-switch solution is compared with the resonant short-circuiting method [19]–[21]. Comparative experiments were performed while transferring 300 watts on a symmetrical series-series DIPT platform using a resistive load and variable frequency inverters around 85 kHz to achieve zero phase angle control. Moreover, analyses of the results are given, and conclusions and perspectives are presented at the end.

Choice and design of the 4Q-Switches

The positioning of the 4Q-switches is presented in Fig. 2. When the switch is in series with an active inverter, it should act as a short circuit and support positive and negative currents. On the other hand, when the switch is in series with an inactive inverter, it should act as an open circuit and support positive and negative induced voltages. Therefore, the choice of a 4Q-switch was made. There are several possible techniques to create a 4Q-switch. This article investigates the use of two technologies: saturable

reactors and IGBT transistors. Using an adequate control circuit, both technologies could achieve the required modes: Low Impedance (LI) mode & High Impedance (HI) mode.

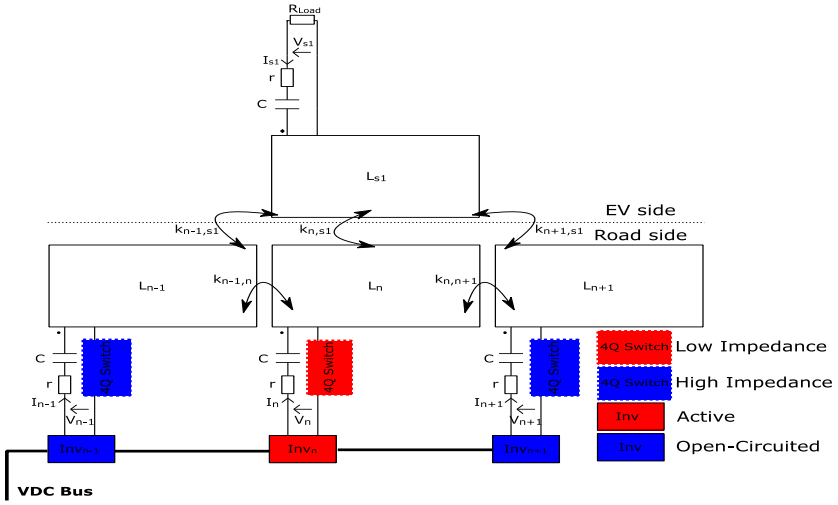

Fig. 2: Using a 4Q-switch with a series-series DIPT system and a resistive load RLoad

The saturable reactor, presented in Fig. 3-a, is a reliable device with low maintenance costs and long life. Its fundamental model is a transformer with two windings: control and power windings. The design used in this article is based on the design presented in [16]. It consists of 2 toroid cores, a control winding, and two power windings in series. This structure doubles the power winding's inductance and protects the control winding from the high induced voltage. A prototype (Fig. 4-a) of the designed saturable inductor is realized based on the specifications presented in Table I.

Table I: Specifications of the realized saturable reactor

Symbol	Definition	Value	Unit
n	Number of turns of the AC winding	8	turns
N	Number of turns of the control winding	210	turns
B_m	Operating peak flux density	1.25	T
A_e	Effective area of the magnetic path	$1.125*10^{-4}$	m^2
l_e	Effective length of the magnetic path	0.102	m
μ_r	Relative permeability of the magnetic core	$3.8*10^4$	/
L_{HI}	Inductance of saturable reactor in High Impedance mode	1.57	mH
L_{LI}	Inductance of saturable reactor in Low Impedance mode	1.01	µH
R_{CW}	DC Resistance of the control winding	4.2	Ω

The chosen topology of the 4Q-switch using the IGBT technology studied in this article is the reverse-blocking IGBT (RB-IGBT) described in [17]. The chosen reverse-blocking, presented in Fig. 3-a, is based on the model developed in [18]. The FGH60N60SMD IGBT module is used with a manual switch to choose between HI-mode or LI-mode (Fig. 4-b). The chosen module has an embedded anti-parallel diode. It has a forward breakdown voltage of 600 V in HI-mode and supports up to 60 A at 100°C in LI-mode, which is sufficient for the intended DIPT application in the experimental phase.

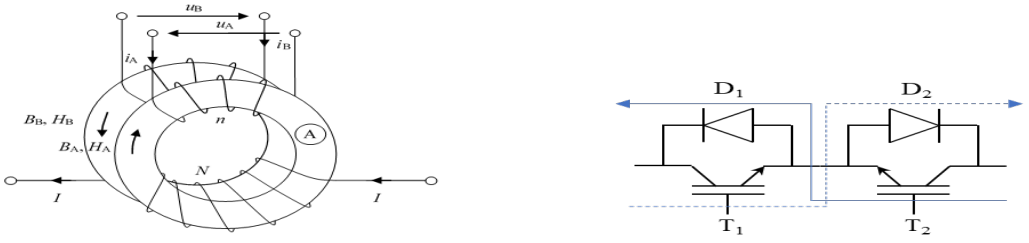

(**a**) (**b**)

Fig. 3: (**a**) Structure of the saturable reactor; (**b**) Structure of the reverse-blocking IGBT 4Q-switch

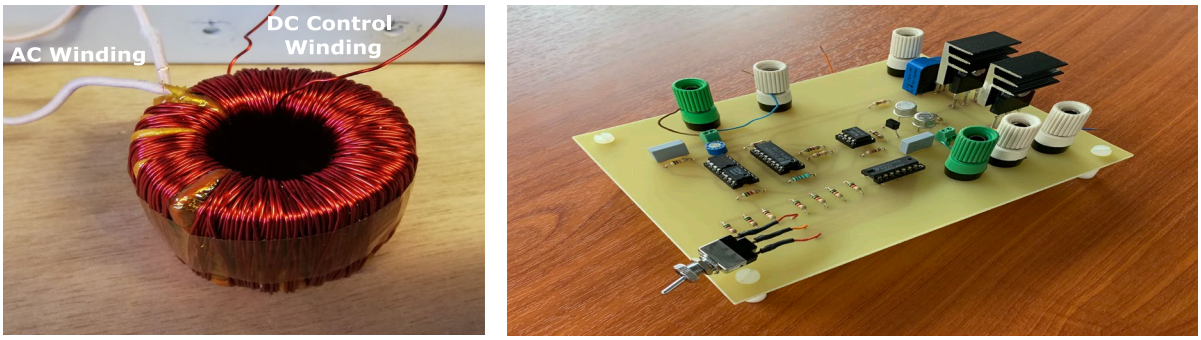

(**a**) Saturable Reactor (**b**) IGBT-RB based on FGH60N60SMD

Fig. 4: Realization of 2 types of saturable reactors

Resonant short circuit mode

Fig. 5 shows the implementation of the Resonant Short Circuit (RSC) mode, proposed in [19] and studied in [20]. The RSC-mode is to short circuit the inverter's output connected to the neighboring inactive coils of the active coil. RSC mode activates the lower two transistors in the H-Bridge and opens the upper ones. Therefore the neighboring inactive coils enter into a series RLC resonant state where the current circulating depends on the induced voltage across the coils and the operating frequency. The advantage of this method is that it does not use any additional components to solve the induced voltage problem across inactive transmitters. However, special care should be taken to limit the resonant current circulating. The active coil cannot operate close to the resonant frequency of the transmitters set to RSC-mode. Otherwise, the current will diverge due to low equivalent impedance. The main added losses to the system using the RSC-mode are due to the dissipation within two turned on transistors (used to achieve the short circuit), the total equivalent series resistance of the coil with the series capacitor, and finally, the magnetic and shielding losses.

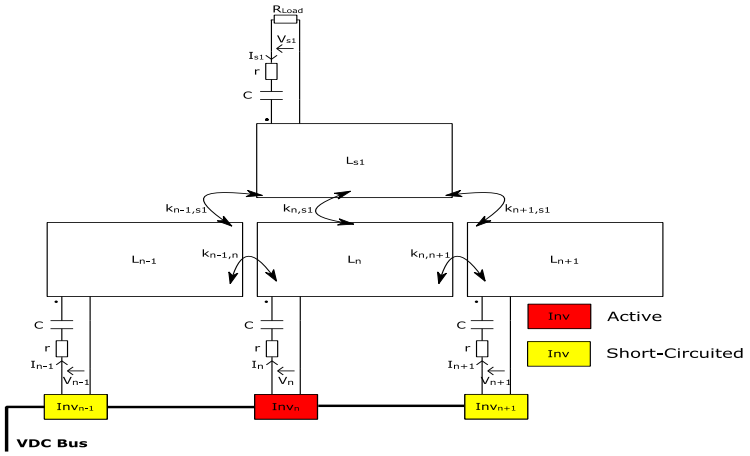

Fig. 5: Using the short-circuiting solution with a series-series DIPT system and a resistive load RLoad

Experimental Results

The three presented methods are compared via a DIPT test bench. The block schematic of the used system is given in Fig. 6-a, and a photo of the test bench is presented in Fig. 6-b. The 3 inverters share topology (full H-bridge) with the same control card containing 1 DSP and 1 FPGA for control and monitoring. IPB017N10N5LF MOSFET modules are used in the H-bridge. The selected DSP (TMS320F28335) manages the system's state machine, the control loop regulation, the PWM control signals, and the communication. The selected FPGA (AGLN250V2-xxGxx) executes the voltage/current phase measurements and manages the PWM control signals sent from the DSP. The DSP is programmed using the compiled code from a Matlab Simulink model using the Texas Instrument C2000 package in Matlab coupled with Code Composer Studio. All tests are done under identical output power (300 W) consumed by a resistive load. Moreover, the active inverter operates at zero current

switching – ZCS (inverter's output voltage and current are in phase). The measurements are done for two positions of the receiver coil, at 0% misalignment ($coil_n$ and $coil_{s1}$ face each other) and 50% misalignment ($coil_{s1}$ is centered between $coil_n$ and $coil_{n+1}$). No lateral misalignment is considered in this study. The values of the system's parameters are given in **Table II**. Fig. 7 shows the induced voltage across the inactive $coil_{n+1}$ when $coil_n$ is activated. The induced peak voltage at 50 % misalignment reaches 80 V, which is considerably higher than the DC bus connected to the input of the inverter. Therefore, it is necessary to adopt one of the three presented solutions to avoid reinjecting power to the DC bus via the anti-parallel diode of the inverter connected to the inactive $coil_{n+1}$.

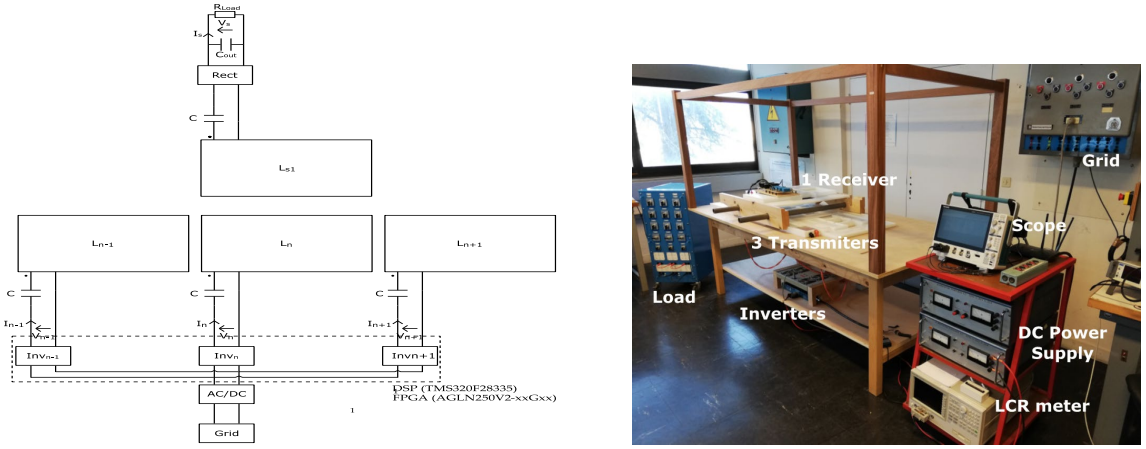

(**a**) (**b**)

Fig. 6: (**a**) Block schematics of the test bench; (**b**) Photo of the test bench

Table II: DIPT Test Bench Parameters

Symbol	Definition	Value	Unit
P_{Load}	Output power consumed by the load	300	W
R_{Load}	Resistive load	3.2 \ 3.7	Ω
V_{DC}	DC bus feeding the inverters	39.6 \ 45.23	V
r	Total equivalent series resistance of the coil & series capacitor	90	mΩ
C	Series compensation capacitor	66	nF
L	Transmitter/Receiver coil's inductance	65	µH
C_{out}	Output capacitor bank	581	µF
f	Operating frequency	83 \ 89	kHz
$k_{n-1,n}$	Coupling between $coil_n$ & $coil_{n-1}$	0.2	%
$k_{n,n+1}$	Coupling between $coil_n$ & $coil_{n+1}$	0.2	%
$k_{n-1,s1}$	Coupling between $coil_{n-1}$ & $coil_{s1}$	4 \ 0	%
$k_{n,s1}$	Coupling between $coil_n$ & $coil_{s1}$	27 \ 17	%
$k_{n+1,s1}$	Coupling between $coil_{n+1}$ & $coil_{s1}$	4 \ 14.6	%

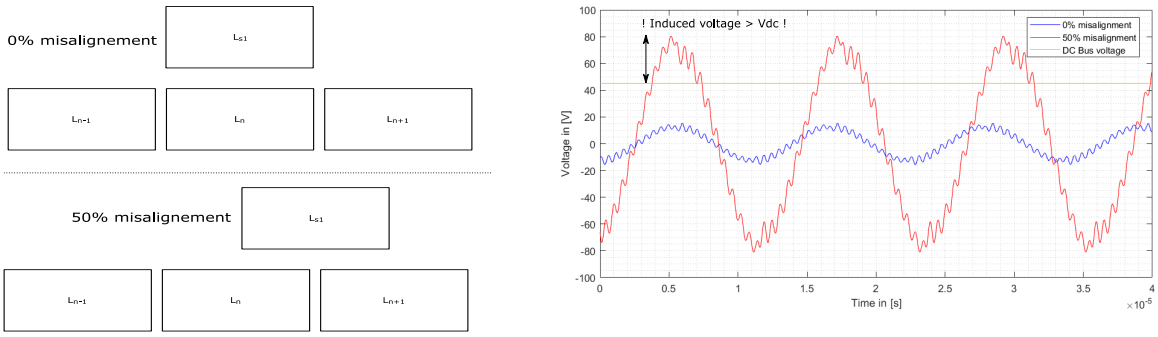

(**a**) (**b**)

Fig. 7: (**a**) 0% vs 50% misalignment; (**b**) Induced voltage across the inactive $coil_{n+1}$ when $coil_n$ is activated

Two saturable reactors have been introduced in the first setup (Fig. 8-a). The first saturable reactor is added in series with the active $coil_n$. At the same time, the second saturable reactor is added in series with the inactive $coil_{n+1}$. In the second setup (Fig. 8-b), we replace the two saturable reactors with RB-IGBT switches and repeat the same measurements under exact conditions. The 4Q-switch, connected in series with the active transmitter, is set to LI-mode. The second switch, connected in series with the inactive transmitter, is set to HI-mode.

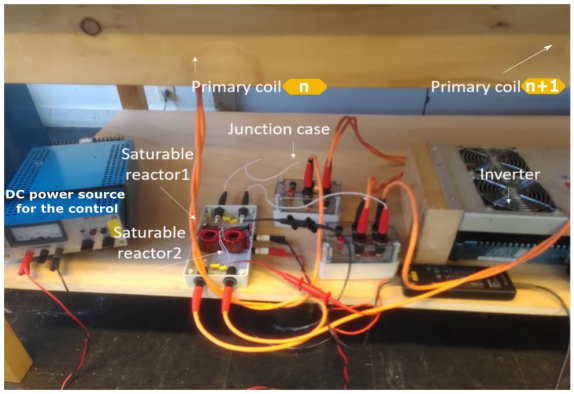

(**a**) Saturable reactor

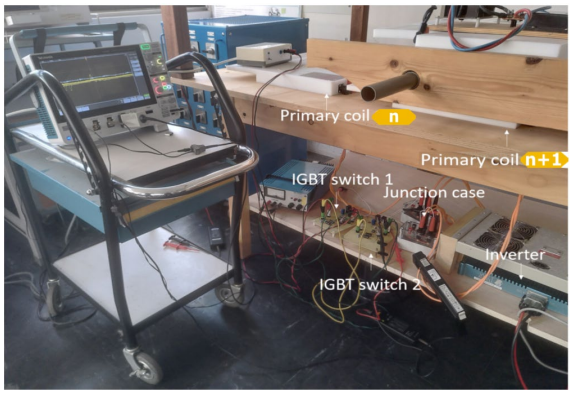

(**b**) IGBT-RB

Fig. 8: 4Q-switches implementation in the platform

In Fig. 9, the voltage and current across the saturable reactor switch in LI-mode are shown in blue. The instantaneous and the average power consumed by the saturable reactor switch are presented in red. The voltage peaks at 20 V, and the current peaks at 13 A for both considered positions (0% and 50% misalignment). We note that voltage leads the current by almost 90° due to the inductive nature of the switch. The total dissipated power by the core and AC winding is the measured average power dissipated over one period: 3.7 W at 0% and 3 W at 50% misalignment. The copper losses in the DC control winding consume 4.2 W. On the other hand, no current was detected circulating across the $coil_{n+1}$ for both considered positions due to the switch in HI-mode. Thus the total losses within the added 2 saturable reactor switches are only due to the one in LI-mode. In Fig. 10, the voltage and current across the RB-IGBT switch in LI-mode are shown in blue. The instantaneous and the average power consumed by the IGBT AC switch are presented in red. The voltage oscillates peaks at 5 V peak and current peaks at 13 A for both considered positions (0% and 50% misalignment). The total dissipated power by LI-mode switch is the measured average power dissipated over one period: 18.7 W at position 0% and 21.8 W at 50% misalignment. The losses in the control circuit are negligible. In addition, no current was detected circulating across the $coil_{n+1}$ for both considered positions due to the switch in HI-mode. Thus the total losses within the added 2 RB-IGBT switches are only due to the one in LI-mode.

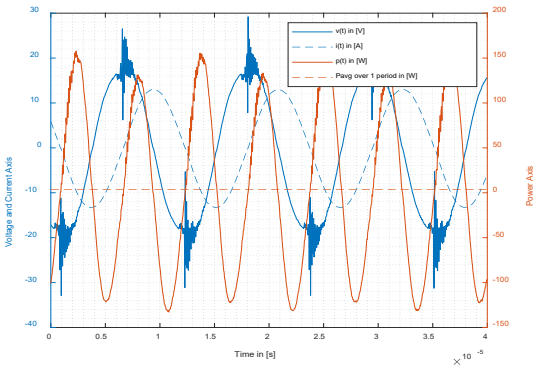

0% misalignment

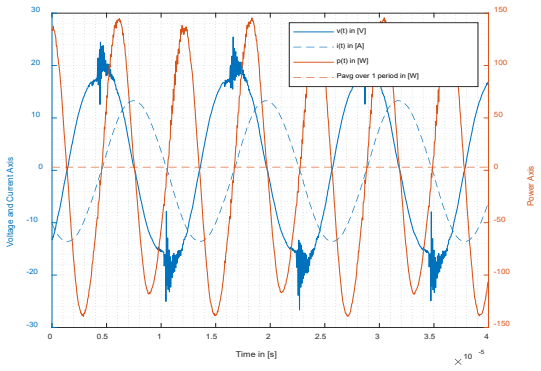

50% misalignment

Fig. 9: Current, voltage, and power loss across the saturable reactor in ON mode

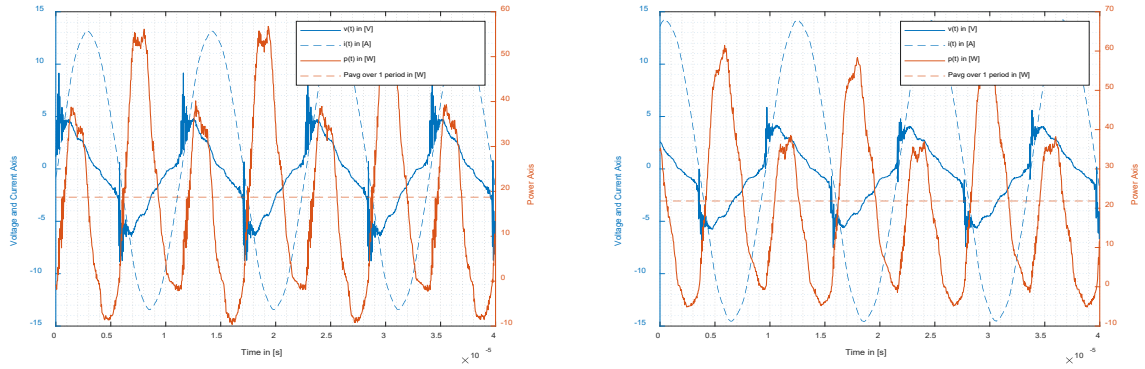

0% misalignment 50% misalignment

Fig. 10: Current, voltage, and power loss across the IGBT-RB Switch in ON mode

The third setup does not need additional 4Q-switches to prevent reinjecting power to the primary DC bus. Instead, the inactive transmitter $coil_{n+1}$ is set to RSC-mode by closing the two lower transistors of the H-bridge $inverter_{n+1}$. In the presence of an induced voltage, the $transmitter_{n+1}$ enters into a series RLC resonant mode. Losses are divided between the inverter in a short circuit (2 transistors conducting at any given time) and the passive RLC components of the transmitter. The total measured equivalent series resistance of the coil and series capacitor at the operating frequency is around 90 mΩ. In Fig. 11, the voltage and current across the $transmiter_{n+1}$ in RSC-mode are presented in blue. The instantaneous and the average power consumed by the $inverter_{n+1}$ are presented in red. At 0% misalignment, the induced voltage across $transmitter_{n+1}$ is very low due to the low magnetic couplings $k_{n,n+1}$, and $k_{n+1,s1}$ at this position. Therefore the current is limited to 1 A peak only. However, at 50% misalignment, the induced voltage across $transmitter_{n+1}$ is much higher due to higher magnetic couplings $k_{n+1,s1}$ at this position. Therefore the current circulating increased to 8.9 A peak. It is noted that the voltage drop across the $inverter_{n+1}$ is relatively low due to the use of transistors with low diode forward voltage and low $RDS_{(ON)}$ (1.7 mΩ). The total dissipated power by the $inverter_{n+1}$ in short-circuit mode is the measured average power dissipated over one period: 0.06 W at position 0 % and 1.18 W at 50 % misalignment. For the total losses in $transmitter_{n+1}$, we add the losses in the RLC equivalent circuit (90 mΩ): 0.06 W at position 0 % and 3.65 W at 50 % misalignment.

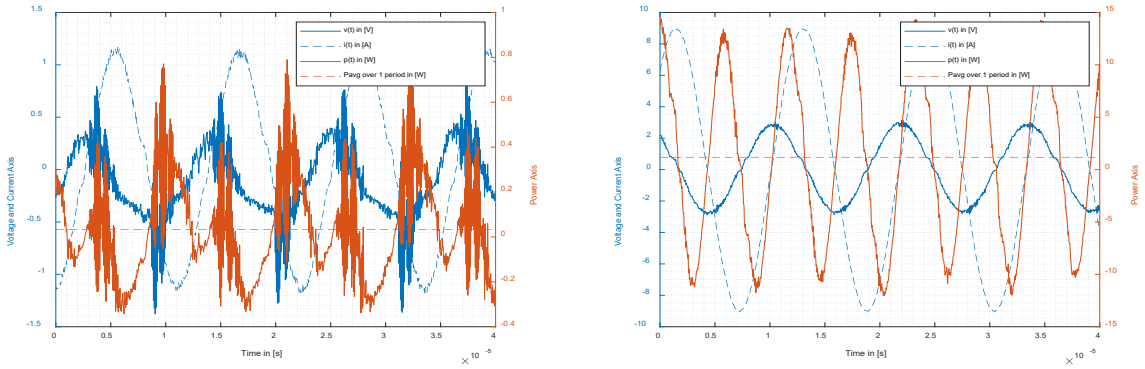

0% misalignment 50% misalignment

Fig. 11: Current, voltage, and power loss across the inverter n+1 in resonant short circuit mode

Comparison and Analysis

The loss comparison of the three tested solutions is shown in

Table III for two positions of the receiver coil. Concerning the two 4Q-switch methods, the presented losses are dissipated by the 4Q-switch in LI-mode located in series with the active $transmiter_n$. On the other hand, the presented losses of the RSC-mode are dissipated within the $transmitter_{n+1}$. All measurements are done with identical power consumed by the load at 300 W and in ZCS mode for the active inverter.

Table III: Losses Comparison

Misalignment	Saturable Reactor 4Q-Switch	IGBT reverse Blocking 4Q-switch	Resonant Short Circuit
0 %	7.9 W	18.7 W	0.12 W
50 %	7.2 W	21.8 W	4.83 W

In LI-mode, a high-frequency current flows through the AC winding, and a constant current flows through the control winding, so there are copper losses in both windings besides the magnetic losses in the core. However, the core operates in the saturation region. Thus, the incremental permeability is small, and the peak variation flux density ΔB_m is also minimal. Therefore, the hysteresis losses are minimal. Furthermore, considering the high resistivity of the chosen Fe-based soft magnetic material, we obtain low losses by eddy currents, leading to low overall core losses. The experimental measurements confirm this remark. There is no control current in high impedance mode, and the high impedance blocks the high-frequency current. Hence, the copper losses in both windings are almost null. Moreover, core losses are also null due to the absence of current circulating in the AC winding.

Under this scenario, the saturable reactor presents fewer losses than the 4Q-switch based on IGBT. However, it is to be noted that the saturable reactor is designed to withstand a 15 A peak current while the chosen IGBT module can withstand 60 A nominal. Moreover, the maximum permissible induced voltage the saturable reactor can withstand is defined by the maximum allowable reinjected current to the DC bus. On the other hand, saturable reactors can support high-temperature variation and are more reliable than semiconductors due to their simplicity and robustness. Heat dissipation is not an issue when the vehicle moves fast across the primary coils. However, an effective thermal dissipation in static applications with higher power transfer (example: during traffic jams). Furthermore, the harsh external environment can also lead to failure. Additional improvement on the saturable reactor could be envisioned by increasing the control's winding number of turns to use a lower control current. This will lower the overall losses of the saturable reactor.

Comparing the RSC mode results with both 4Q-switch methods, we observe significantly fewer losses and lower costs since no additional elements are required. The lower losses are mainly due to the geometry of the coils used. The used geometry in the DIPT platform has a very low magnetic coupling between transmitter coils. Therefore, the induced voltage on the neighboring inactive transmitter coil was relatively limited. Thus the current circulating in the transmitter in RSC mode was also limited, explaining the lower losses. For this reason, the losses of the RSC mode solution are highly dependent on the choice of the geometry for the transmitter and receiver coils, unlike the 4Q-switch methods with fixed losses proportional to the transmitted power.

Conclusions and Perspectives

This article compares several solutions for high induced voltage across inactive transmitting coils in a series-series compensation DIPT system. A 4Q-switch is presented and realized based on two technologies: Saturable reactors and IGBT transistors. The 4Q-switch solution is compared with the short-circuiting method. Experimental validation is performed on a series-series DIPT platform by transferring a 300 W to a resistive load at a variable frequency control between 83 kHz and 89 kHz. Results show that the saturable reactor presents fewer losses than the 4Q-switch based on IGBT. Moreover, the 4Q-switch offers better reliability and overvoltage withstand. On the other hand, tests also showed that the RSC-mode dissipated less power with no added costs. However, the losses in RSC-mode depend on the coils' chosen geometry. In further research, a comparison between the three solutions will be performed at higher power transfer (several kW) using several coil geometries. Moreover, increasing the number of turns of the control windings for the saturable reactor, thus using lower control current, results in lower losses.

References

[1] F. Un-Noor, S. Padmanaban, L. Mihet-Popa, M. Mollah, and E. Hossain, "A Comprehensive Study of Key Electric Vehicle (EV) Components, Technologies, Challenges, Impacts, and Future Direction of Development," *Energies*, vol. 10, no. 8, p. 1217, Aug. 2017, doi: 10.3390/en10081217.

[2] G. A. Covic and J. T. Boys, "Modern Trends in Inductive Power Transfer for Transportation Applications," *IEEE J. Emerg. Sel. Top. Power Electron.*, vol. 1, no. 1, pp. 28–41, Mar. 2013, doi: 10.1109/JESTPE.2013.2264473.

[3] R. Bosshard and J. W. Kolar, "Inductive power transfer for electric vehicle charging: Technical challenges and tradeoffs," *IEEE Power Electron. Mag.*, vol. 3, no. 3, pp. 22–30, Sep. 2016, doi: 10.1109/MPEL.2016.2583839.

[4] L. Hutchinson, B. Waterson, B. Anvari, and D. Naberezhnykh, "Potential of wireless power transfer for dynamic charging of electric vehicles," *IET Intell. Transp. Syst.*, vol. 13, no. 1, pp. 3–12, Jan. 2019, doi: 10.1049/iet-its.2018.5221.

[5] G. Duarte, A. Silva, and P. Baptista, "Assessment of wireless charging impacts based on real-world driving patterns: Case study in Lisbon, Portugal," *Sustain. Cities Soc.*, vol. 71, p. 102952, Aug. 2021, doi: 10.1016/j.scs.2021.102952.

[6] N. Liu and T. G. Habetler, "Design of a Universal Inductive Charger for Multiple Electric Vehicle Models," *IEEE Trans. Power Electron.*, vol. 30, no. 11, pp. 6378–6390, Nov. 2015, doi: 10.1109/TPEL.2015.2394734.

[7] K. Aditya and S. S. Williamson, "Comparative study of series-series and series-parallel topology for long track EV charging application," in *2014 IEEE Transportation Electrification Conference and Expo (ITEC)*, Dearborn, MI, Jun. 2014, pp. 1–5. doi: 10.1109/ITEC.2014.6861793.

[8] Y. Chen, H. Zhang, C.-S. Shin, K.-H. Seo, S.-J. Park, and D.-H. Kim, "A Comparative Study of S-S and LCC-S Compensation Topology of Inductive Power Transfer Systems for EV Chargers," in *2019 IEEE 10th International Symposium on Power Electronics for Distributed Generation Systems (PEDG)*, Xi'an, Jun. 2019, pp. 99–104. doi: 10.1109/PEDG.2019.8807684.

[9] J. L. Villa, J. Sallán, A. Llombart, and J. F. Sanz, "Design of a high frequency Inductively Coupled Power Transfer system for electric vehicle battery charge," *Appl. Energy*, vol. 86, no. 3, pp. 355–363, Mar. 2009, doi: 10.1016/j.apenergy.2008.05.009.

[10] "ICNIRP GUIDELINES FOR LIMITING EXPOSURE TO TIME-VARYING ELECTRIC AND MAGNETIC FIELDS (1 Hz TO 100 kHz)," *Health Phys.*, vol. 99, no. 6, pp. 818–836, Dec. 2010, doi: 10.1097/HP.0b013e3181f06c86.

[11] K. Kim and J.-W. Choi, "Influences of Magnetic Couplings in Transmitter Array of MIMO Wireless Power Transfer System," in *2019 IEEE Wireless Power Transfer Conference (WPTC)*, London, United Kingdom, Jun. 2019, pp. 531–535. doi: 10.1109/WPTC45513.2019.9055594.

[12] F. Lu, H. Zhang, H. Hofmann, and C. C. Mi, "A Dynamic Charging System With Reduced Output Power Pulsation for Electric Vehicles," *IEEE Trans. Ind. Electron.*, vol. 63, no. 10, pp. 6580–6590, Oct. 2016, doi: 10.1109/TIE.2016.2563380.

[13] A. Pacini, A. Costanzo, S. Aldhaher, and P. D. Mitcheson, "Load- and Position-Independent Moving MHz WPT System Based on GaN-Distributed Current Sources," *IEEE Trans. Microw. Theory Tech.*, vol. 65, no. 12, pp. 5367–5376, Dec. 2017, doi: 10.1109/TMTT.2017.2768031.

[14] G. A. Covic, M. L. G. Kissin, D. Kacprzak, N. Clausen, and H. Hao, "A bipolar primary pad topology for EV stationary charging and highway power by inductive coupling," in *2011 IEEE Energy Conversion Congress and Exposition*, Phoenix, AZ, USA, Sep. 2011, pp. 1832–1838. doi: 10.1109/ECCE.2011.6064008.

[15] P. Mali, *Magnetic amplifiers: principles and applications.* New York: J.F. Rider, 1960.

[16] M. S. Perdigao, M. F. Menke, A. R. Seidel, R. A. Pinto, and J. M. Alonso, "A Review on Variable Inductors and Variable Transformers: Applications to Lighting Drivers," *IEEE Trans. Ind. Appl.*, vol. 52, no. 1, pp. 531–547, Jan. 2016, doi: 10.1109/TIA.2015.2483580.

[17] C. Benboujema, A. Schellmanns, N. Batut, J. B. Quoirin, and L. Ventura, "Low losses bidirectional switch for AC mains," p. 10.

[18] A. Trentin, L. de Lillo, L. Empringham, P. Wheeler, and J. Clare, "Experimental Comparison of a Direct Matrix Converter Using Si IGBT and SiC MOSFETs," *IEEE J. Emerg. Sel. Top. Power Electron.*, vol. 3, no. 2, pp. 542–554, Jun. 2015, doi: 10.1109/JESTPE.2014.2381001.

[19] A. Caillierez, D. Sadarnac, A. Jaafari, and S. Loudot, "Dynamic inductive charging for electric vehicle: modelling and experimental results," p. 1.7.01-1.7.01, Jan. 2014, doi: 10.1049/cp.2014.0423.

[20] P.-A. Gori, D. Sadarnac, A. Caillierez, and S. Loudot, “Sensorless inductive power transfer system for electric vehicles: Strategy and control for automatic dynamic operation,” in *2017 19th European Conference on Power Electronics and Applications (EPE’17 ECCE Europe)*, Warsaw, Sep. 2017, p. P.1-P.10. doi: 10.23919/EPE17ECCEEurope.2017.8099233.

[21] W. Kabbara, M. Bensetti, T. Phulpin, A. Caillierez, S. Loudot, and D. Sadarnac, “A Control Strategy to Avoid Drop and Inrush Currents during Transient Phases in a Multi-Transmitters DIPT System,” *Energies*, vol. 15, no. 8, Art. no. 8, Jan. 2022, doi: 10.3390/en15082911.